ACS APPLIED MATERIALS & INTERFACES

Research Article

www.acsami.org

Photoactive Hybrid Material Based on Pyrene Functionalized PbS Nanocrystals Decorating CVD Monolayer Graphene

Chiara Ingrosso,*[,†] Giuseppe V. Bianco,[§] Michela Corricelli,[†,⊥] Roberto Comparelli,[†] Davide Altamura,[∥] Angela Agostiano,[†,⊥] Marinella Striccoli,[†] Maria Losurdo,[§] M. Lucia Curri,[†] and Giovanni Bruno[§]

[†]CNR-IPCF sez. Bari, c/o Dipartimento di Chimica, Universitàdi Bari, via Orabona 4-I 70126 Bari, Italy

[§]CNR-IMIP, c/o Dipartimento di Chimica, Università di Bari, via Orabona 4-I 70126 Bari, Italy

[∥]CNR-IC, via Amendola 122/O-I 70126 Bari, Italy

[⊥]Dipartimento di Chimica, Università di Bari, via Orabona 4-I 70126 Bari, Italy

Supporting Information

ABSTRACT: A simple and facile solution-based procedure is implemented for decorating a large area, monolayer graphene film, grown by chemical vapor deposition, with size-tunable light absorbing colloidal PbS nanocrystals (NCs). The hybrid is obtained by exposing a large area graphene film to a solution of 1-pyrene butyric acid surface coated PbS NCs, obtained by a capping exchange procedure onto presynthesized organic-capped NCs. The results demonstrate that at the interface, multiple and cooperative $\pi-\pi$ stacking interactions promoted by the pyrene ligand coordinating the NC surface lead to a successful anchoring of the nano-objects on the graphene platform which concomitantly preserves its aromatic structure. Interligand interactions provide organization of the nano-objects in highly interconnected nanostructured multilayer coatings, where the NCs retain geometry and composition. The resulting hybrid exhibits a sheet resistance lower than that of bare graphene, which is explained in terms of electronic communication in the hybrid, due to the interconnection of the NC film and to a hole transfer from photoexcited PbS NCs to graphene, channelled at the interface by pyrene. Such a direct electron coupling makes the manufactured hybrid material an interesting component for optoelectronics, sensors and for optical communication and information technology.

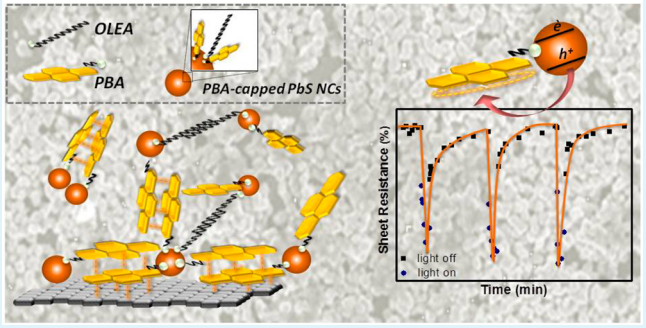

KEYWORDS: *CVD monolayer graphene, colloidal PbS NCs, photoactive hybrid material*

1. INTRODUCTION

Since its first isolation in 2004,[1] graphene, a one-atom thick two-dimensional monolayer of sp_2 hybridized carbon atoms organized in a honeycomb lattice, has represented an extraordinarily attractive component of sensors, solar cells, supercapacitors, batteries and nanocomposites[2−5] due to its unique properties as high conductivity for charge carriers, light transparency from visible to infrared, excellent thermal conductivity, high surface area, good biocompatibility, and mechanical flexibility.

Two-dimensional graphene platforms possess a high reactivity which opens venue to a large variety of strategies of hybridization by means of molecular decoration approaches both for enhancing its pristine functionalities and for conveying novel properties,[6,7] thus extending its potential for diverse advanced technological applications.

Decoration of graphene with colloidal inorganic nanocrystals (NCs) allows the preparation of hybrid materials with original properties, since it allows the combination of the outstanding functionalities of the organic compound with the original size-dependent properties of the nanosized inorganic matter. Indeed, nanocrystals and nanoparticles, with their unique fundamental properties, have been widely exploited in a plethora of fields, such as electronics, energy conversion and environmental and life science.[8,9] Colloidal NCs, prepared by means of solution-based colloidal chemistry routes, are particularly interesting for chemically decorating graphene, because their surface is coordinated by a layer of surfactant molecules, whose chemistry can be tuned by implementing suitable ligand exchange procedures, and allow to immobilize nanoparticles on diverse surfaces for manufacturing hybrids or hierarchical structures that exhibit the functionalities of nanosized matter on mesoscale, promising for device applications.[10]

Recently, hybrid materials formed of semiconductor NCs supported on graphene sheets, have been investigated for their integration in solar cells, sensors, (bio)imaging, and photodetectors.[11−14] In such nanocomposites, when the interface

Received: November 26, 2014
Accepted: February 4, 2015
Published: February 16, 2015

DOI: 10.1021/am5081925
ACS Appl. Mater. Interfaces 2015, 7, 4151−4159

between NCs and graphene is properly designed for allowing electron coupling between the components, charge transfer processes from the photoexcited NCs to the aromatic compound have been observed,[15] resulting in a hybrid having a photoresponse ranging from visible to infrared and a conductivity increased with respect to that of bare graphene.[11,12]

Diverse approaches have been implemented for manufacturing hybrids based on semiconductor NCs and graphene. One method relays on the in situ synthesis of both nanoparticles and graphene, starting from graphene oxide and inorganic precursors of the nano-objects. The latter nucleate and grow directly onto graphene oxide, which concomitantly goes to reduced graphene oxide.[14] Other methods provide the in situ synthesis of nanoparticles from precursors, directly on preexisting graphene sheets.[13]

Although such routes result into hybrids whose components can be interfaced by linker molecules or even in close contact, the obtained materials exhibit an intrinsic low crystallinity,[16] which may result detrimental for the final optoelectronic properties of the hybrid.

These downsides can be effectively overcome by using an ex-situ approach, in which presynthesized highly crystalline colloidal NCs are bound by means of a molecular linker to highly crystalline graphene. Thioglycolic acid-capped CdTe NCs have been immobilized on mono- and few-layer exfoliated graphene flakes by using trimethyl (2-oxo-2-pyrene-1-ylethyl)-ammonium bromide as a linker, which anchors non covalently graphene by tight $\pi-\pi$ stacking interactions, not affecting the conjugated sp_2 carbon atom network and it acts as channel for electron transfers between the hybrid components.[17]

In our work, ex-situ synthesized high quality colloidal PbS NCs, directly surface coordinated by a functionalized pyrene capping ligand, have been anchored on large area monolayer graphene film, fabricated by chemical vapor deposition (CVD). Among the main methodologies developed for graphene synthesis (mechanical and chemical exfoliation of graphite/graphite oxide, epitaxial growth by thermal decomposition of silicon carbide and CVD growth on catalytic metal substrates), CVD offers the advantage of being a low cost and scalable production method suited for electron industry. Moreover, CVD graphene can be transferred onto a wide range of substrates providing enhanced technological opportunities.[18] PbS NCs have been selected because of their unique features as size-dependent absorption in the infrared spectral range, narrow and tunable photoluminescence and high photostability.

A hybrid material based on oleic acid (OLEA)-capped PbS NCs and exfoliated graphene has been recently tested as active material of a photodetector exhibiting a photoresponse in the visible and infrared spectra region.[11,12]

Here, a surface capping exchange procedure has been performed on oleic acid (OLEA) and trioctyphosphine (TOP) coated PbS NCs for functionalizing them by 1-pyrene butyric acid (PBA), resulting in stable and optically transparent solutions, where the nano-objects preserve their size, shape and unique optical properties. Then the CVD graphene film, supported on SiO_2/Si substrates, has been decorated with the colloidal PbS NCs by incubation in a dispersion of the NCs, directly surface coordinated by PBA. Such a short chain aromatic ligand is able to coordinate the PbS NC surface by means of its carboxylic functionality and to chemically bind the NCs, which result also electrically interconnected by interligand interactions, to graphene by $\pi-\pi$ interactions promoting at the interface electron transfer between the two hybrid components.

The manufactured hybrid system has been characterized by spectroscopy and microscopy techniques, as well as by Hall measurements. The investigation demonstrates a stable anchoring of the PbS NCs in highly interconnected multilayers on graphene, with retention of geometry and composition. After functionalization, graphene preserves its sp_2 carbon atom density, resulting in a p-doped increased conductivity on large area, due to transfer of holes from the photoexcited NCs channeled by pyrene. Such properties make the prepared hybrid material very suited for integration in solar cells, photodetectors, (bio)sensors, imaging, and communication systems.

2. MATERIALS AND METHODS

2.1. Materials. 1-Pyrene butyric acid, lead(II) oxide (PbO, powder 99.99%), hexamethyldisilathiane (HMDS, synthesis grade), trioctylphosphine (TOP, 90% technical grade), methanol (≥99.8%) and chloroform (≥99.8%) were purchased by Sigma-Aldrich and used as received. 1-Octadecene (ODE, 90% technical grade) and oleic acid (OLEA, technical grade 90%), also purchased by Sigma-Aldrich, were distilled before use.

2.2. Methods. *2.2.1. Synthesis of OLEA/TOP-Capped PbS NCs.* The preparation of PbS NCs was carried out as previously reported.[19] In a typical synthesis, 4 mmol of PbO, 3.0 mL of trioctylphosphine (TOP), and 2.3 mL of oleic acid (OLEA) were added to 36 mL of 1-octadecene (ODE) and stirred under vacuum at 120 °C. Then, a 20 mM solution of sulfur precursor, hexamethyldisilathiane (HMDS) in ODE, was rapidly injected, followed by fast cooling at room temperature. The obtained NCs were purified by centrifugation by adding to the reaction product a large amount of ethanol and the precipitate was then dispersed in chloroform.

2.2.2. Capping Exchange of OLEA/TOP-Capped PbS NCs with 1-Pyrene Butyric Acid (PBA). The ligand exchange process was typically carried out under inert atmosphere. First, the as synthesized PbS NCs were repeatedly washed with methanol to remove the excess of organic ligand coordinating the NC surface. Chloroform dispersions of BPA capping ligand were added to the washed 10^{-2} M PbS NC chloroform solutions in 1:5 PbS/PBA molar ratio and the mixture was left to stir overnight at room temperature. The NCs were then washed with methanol or acetonitrile to remove the aromatic ligand in excess and then redispersed in chloroform for further studies. Concentrated transparent solutions of PBA-capped PbS NCs can be obtained (10^{-2} M), that are stable over months without further addition of PBA molecules.

2.2.3. Graphene Growth by Chemical Vapor Deposition (CVD). Monolayer graphene with 50−110 μm^2 grain sizes (see Figure S1 of Supporting Information) was grown by CVD on 25 μm thick copper foils (Alfa Aesar, item no. 13382) in a typical quartz tube CVD reactor at 1000 °C using CH_4/H_2 as precursors.

The prepared graphene was then transferred onto 300 nm SiO_2/Si substrate by using a thermal release tape and a water solution of ammonium persulfate (0.1 M) as copper etchant. Before graphene transfer, the SiO_2/Si substrates were treated with O_2 plasma for improving adhesion.

The graphene transferred on SiO_2/Si substrate were finally dipped in toluene/ethanol/anisole (1/1/1) solution for removing any organic impurities of thermal tape traces.

2.2.4. Functionalization of CVD Grown Graphene with 1-Pyrene Butyric Acid (PBA)-Coated PbS NCs. Large area monolayer graphene transferred on SiO_2/Si substrate was incubated in a 5×10^{-3} M chloroform solution of PBA-capped PbS NCs overnight and then rinsed with chloroform to remove the NCs not specifically adsorbed.

2.3. Characterization. Steady state UV−Vis absorption spectra were recorded with a Cary 5000 (Varian) UV/vis/NIR spectrophotometer. Steady state photoluminescence spectra were recorded by using a Fluorolog 3 spectrofluorimeter (HORIBA Jobin−Yvon),

DOI: 10.1021/am5081925
ACS Appl. Mater. Interfaces 2015, 7, 4151−4159

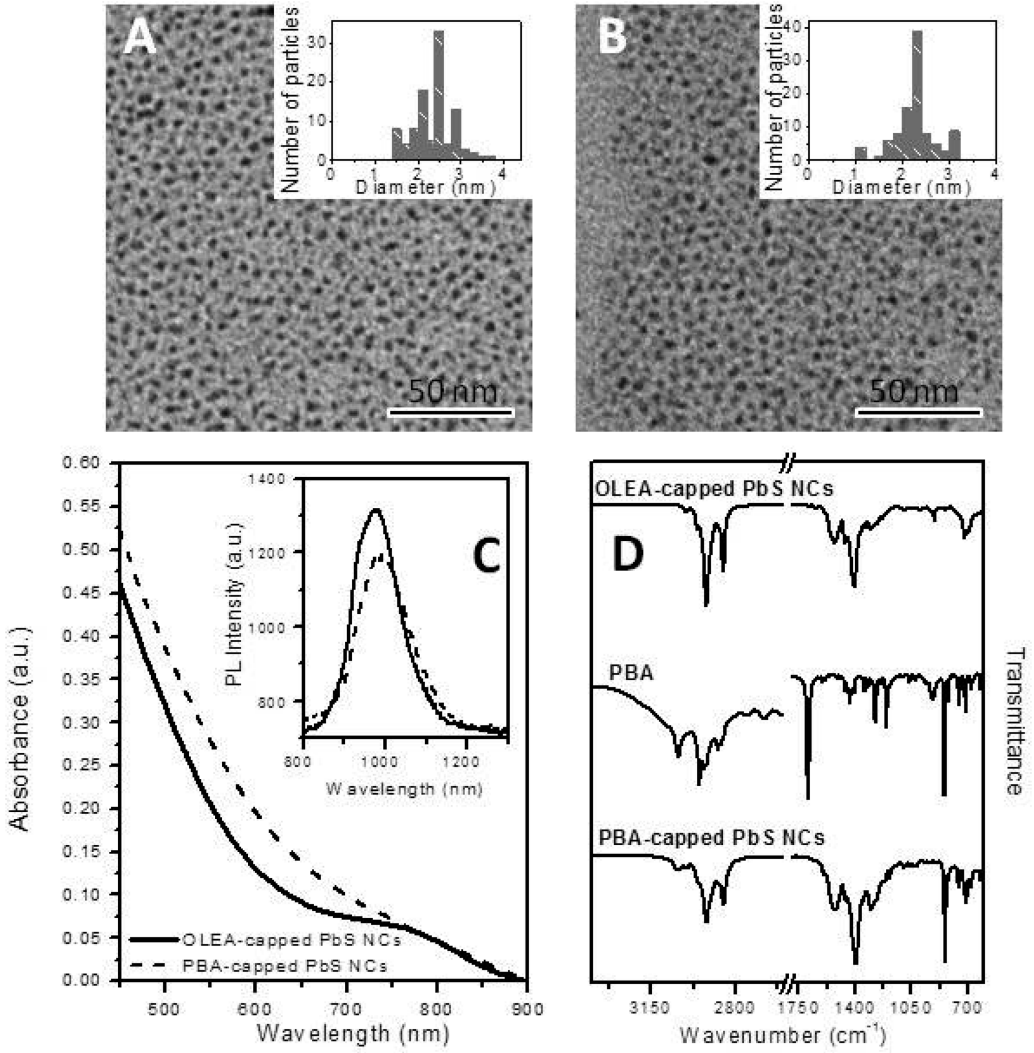

Figure 1. TEM micrographs of OLEA/TOP-capped (A) and PBA-coated (B) PbS NCs with corresponding size statistical analysis. (C) Steady state UV−vis-NIR absorption and photoluminescence (PL) spectra of PbS NCs before and after capping exchange. (D) ATR-FTIR spectra of OLEA/TOP-capped PbS NCs, bare PBA and PBA-coated PbS NCs.

equipped with double grating excitation and emission monochromators. All optical measurements were performed at room temperature.

Midinfrared spectra were acquired with a Varian 670-IR spectrometer equipped with a DTGS (deuterated tryglycine sulfate) detector. The spectral resolution used for all experiments was 4 cm^{-1}. For attenuated total reflection (ATR) measurements, the internal reflection element (IRE) used was a one-bounce 2 mm diameter diamond microprism. Cast films have been prepared directly onto the internal reflection element, by depositing the solution or suspension of interest (3−5 μL) on the upper face of the diamond crystal and allowing the solvent to evaporate.

Graphene Raman spectra were collected using a LabRAM HR Horiba-Jobin Yvon spectrometer with a 473 and 532 nm excitation laser sources to minimize the fluorescence emission of copper and SiO_2/Si substrates, respectively. Measurements were carried out under ambient conditions at low laser power (1 mW) to avoid laser-induced damage. The Raman band recorded from a silicon wafer at 520 cm^{-1} was used to calibrate the spectrometer, and the accuracy of the spectral measurement was estimated to be 1 cm^{-1}.

TEM analyses were performed by using a Jeol Jem-1011 microscope, operated at 100 kV. TEM images were acquired by a Quemesa Olympus CCD 11 Mp Camera. The samples were prepared by dipping the 300 mesh amorphous carbon-coated Cu grid in chloroform solution of PbS NCs and leaving the solvent to dry. Size statistical analysis (NP average size and size distribution) of the samples were performed by freeware ImageJ analysis program. At least 150 NCs were counted for each sample.

X-ray powder diffraction (XRPD) patterns were collected at room temperature by means of a Rigaku RINT2500 rotating anode laboratory diffractometer (50 kV, 200 mA) equipped with a silicon strip Rigaku D/teX Ultra detector. An asymmetric Johansson Ge(111) crystal was used to select the monochromatic Cu Kα1 radiation (λ = 1.54056 Å). The measurements were executed in transmission mode, by introducing the sample in a 0.3 mm Lindemann glass capillary mounted on the axis of the goniometer.

Field emission scanning electron microscopy (FE-SEM) was performed by a Zeiss Sigma microscope operating in the range 0.5−20 kV and equipped with an in-lens secondary electron detector and an INCA Energy Dispersive Spectroscopy (EDS) detector. FE-SEM samples were prepared by suspending in methanol a proper amount of catalyst powder and casting a drop of the obtained suspension onto a silicon slide. Samples were mounted onto stainless-steel sample holders by double-sided carbon tape and grounded by silver paste.

Topography an phase mode AFM measurements were performed in air and at room temperature, by means of a PSIA XE-100 SPM system operating in tapping mode. A silicon SPM sensor for noncontact AFM (Park Systems), having a spring constant of 42 N m^{-1} and a resonance frequency of 330 kHz, was used. Micrographs were collected on six distinct areas of samples, with a scan size area of 2 μm × 2 μm, by sampling the surface at a scan rate within 1.0−0.5 Hz and a resolution

DOI: 10.1021/am5081925
ACS Appl. Mater. Interfaces 2015, 7, 4151−4159

of 256 × 256 pixels. Topography AFM images were processed by using the XEI software to obtain statistical data.

2.3.1. Electrical Measurements. Four gold contacts were evaporated on graphene through holes in a mask used for electron microscopy; this approach was used to avoid any possible complication arising from unintentional doping that may stem from exposure of graphene to lithography chemicals. The sample was then loaded in the Hall system (MMR Technologies, Inc.) equipped with a temperature controlled sample holder set at 200 K and a pumping system to reach a base vacuum of 10^{-4} Torr. Electrical measurements were carried out using a four-point contacts geometry in the Van der Pauw configuration on a sampled area of 5 × 5 mm^2. The hybrid material was illuminated by a white light LED source trough an optical window of sample holder.

3. RESULTS AND DISCUSSION

Oleic acid (OLEA)- and trioctylphosphine (TOP)-coated PbS NCs have been synthesized by the colloidal chemistry route reported in[19] and then functionalized by a capping exchange procedure with pyrene-1-butyrric acid (PBA). This aromatic molecule is typically used as multifunctional anchoring system for carbon based allotropic forms.[17] Similarly here, it is expected to link the nano-objects, which coordinates by its end carboxyl functionality, to the graphene platform, by means of $\pi-\pi$ interactions.

Microscopy and spectroscopy measurements have been performed for investigating geometry, optical properties, surface chemistry and crystalline structure of the PbS NCs, before and after treatment with PBA ligand, to assess the NC surface chemistry modification, as well as retention of the intrinsic NC properties.

Figure 1 shows TEM micrographs, UV−vis-NIR, and FTIR-ATR spectra of the PbS NCs coordinated by pristine OLEA/TOP ligands and by PBA after surface treatment.

The TEM micrograph of panel A displays round-shaped nano-objects well dispersed on the grid because of the surface coordination with the long alkyl chain OLEA/TOP molecules. The statistical analysis of the average size and size distribution, reported in the some panel, allows to estimate a mean size of 2.3 ± 0.5 nm for the OLEA/TOP-caoted PbS NCs. After treatment with PBA, no detectable change in morphology of the PbS NCs is observed and the average size and size distribution of the nano-objects are retained (panel B of Figure 1).

The UV−vis−NIR absorption spectrum of the OLEA/TOP-capped PbS NCs (Panel C of Figure 1) shows a peak at ∼780 nm ascribed to the first allowed exciton transition, as reported for 2.3 nm sized NCs,[20] that matches with the mean value estimated by TEM investigation (panel A of Figure 1). The photoluminescence spectrum of the OLEA/TOP-capped PbS NCs (inset of panel C) is characterized by the presence of a narrow emission peak, Stoke's shifted up to 975 nm and with a full-width at half-maximum (fwhm) equal to 175 meV accounting for the narrow size distribution of the NCs. Such an emission peak can be attributed to the band-edge recombination process, whereas no emission signal ascribed to defect states typically located on low energy side is observed.

After processing with PBA, the absorption spectrum significantly broadens, and it presents a shoulder monotonically increasing toward the higher energy side of the spectrum. In addition, the fwhm of the photoluminescence peak increases up to 220 meV, its intensity is slightly quenched with respect to that of pristine OLEA/TOP-capped PbS NCs and its maximum red-shifs toward the lower energy side, namely at 983 nm (panel C of Figure 1).

The broadening of the absorption and emission peak, the red-shift and slight quenching of the PL peak can be ascribed to the appearance or redistribution of the NC midgap surface defect states,[21] occurring as a consequence of ligand reorganization, upon desorption of OLEA and TOP ligands and coordination of the new capping agent after treatment with PBA.[22] On the other hand, oxidation of the NC surface due to treatment with PBA can be ruled out, as in that case a blue-shift of the exciton peak would have been observed.[23] The appearance of the unstructured absoption spectrum after PBA treatment can be explained considering that surface related charge separation and polarization effects can arise in the treated NCs, known to be sensitive to the π ring system of pyrene molecules.[24]

Panel D of Figure 1 compares the infrared spectra of the PBA-coated PbS NCs with those recorded from the pristine OLEA/TOP-capped PbS NCs and from bare PBA.

The high wavenumber region of the spectrum of PBA-capped PbS NCs is characterized by the presence of typical signals of both PBA and OLEA/TOP ligand molecules. Namely, at 3037 cm^{-1} the aromatic C−H stretching vibration of pyrene molecule is evident, along with the weak, but definite band of the olefinic C−H stretching of OLEA at 3008 cm^{-1} and the weak asymmetric $-CH_3$ stretching and the strong asymmetric and symmetric stretching of $-CH_2-$ of OLEA and TOP at around 2954, 2919, and 2850 cm^{-1}, respectively.

In regards of the spectral region at lower wavenumbers, at 1525 and 1401 cm^{-1}, the signals of the antisymmetric and symmetric COO^- stretching, respectively coordinated to surface Pb atoms are evident. The lack of the free C═O stretching band of the PBA molecule expected at 1691 cm^{-1} excludes the presence of uncoordinated PBA molecules, free in solution of the PBA-capped PbS NCs. On the contrary, evidence of the presence of PBA molecules coordinated to the surface of the PbS NCs is given by the strong band pointed at 844 cm^{-1}, assigned to the characteristic out of plane C−H bending of pyrene aromatic ring. At lower wavenumbers, signals due to the combination of the aromatic and alkylic skeletal C−C bending with the methylene C−H bending are evident in the spectrum of PBA-coated PbS NCs.

FTIR measurements confirm the coordination of the new pyrene based ligand at the surface of the nano-objects along with a concomitant partial retention of the pristine ligands coordinated to the surface of the PbS NCs, after performing one step ligand exchange. It is worthwhile to notice that multiple ligand exchange procedures have been also tested in order to increase the ligand replacement yield. However, such treatments lead to a decrease of the stability of the NC colloidal solution with concomitant aggregation phenomena limiting NC processability from solution and induce surface defect states, which detrimentally affect the optoelectronic properties of the NCs.[25]

Figure S2 of Supporting Information compares XRPD patterns of OLEA- and PBA-capped PbS NCs with reference pattern of rock-salt PbS crystalline phase. The image shows that the profiles of the PbS NCs, before and after treatment with PBA, can be both indexed as diffraction from the rock-salt PbS phase,[19] and differ just for contribution of background, as expected for a different capping, thus demonstrating that the crystalline nature of the nano-objects is unaffected by the capping exchange process.

DOI: 10.1021/am5081925
ACS Appl. Mater. Interfaces 2015, 7, 4151−4159

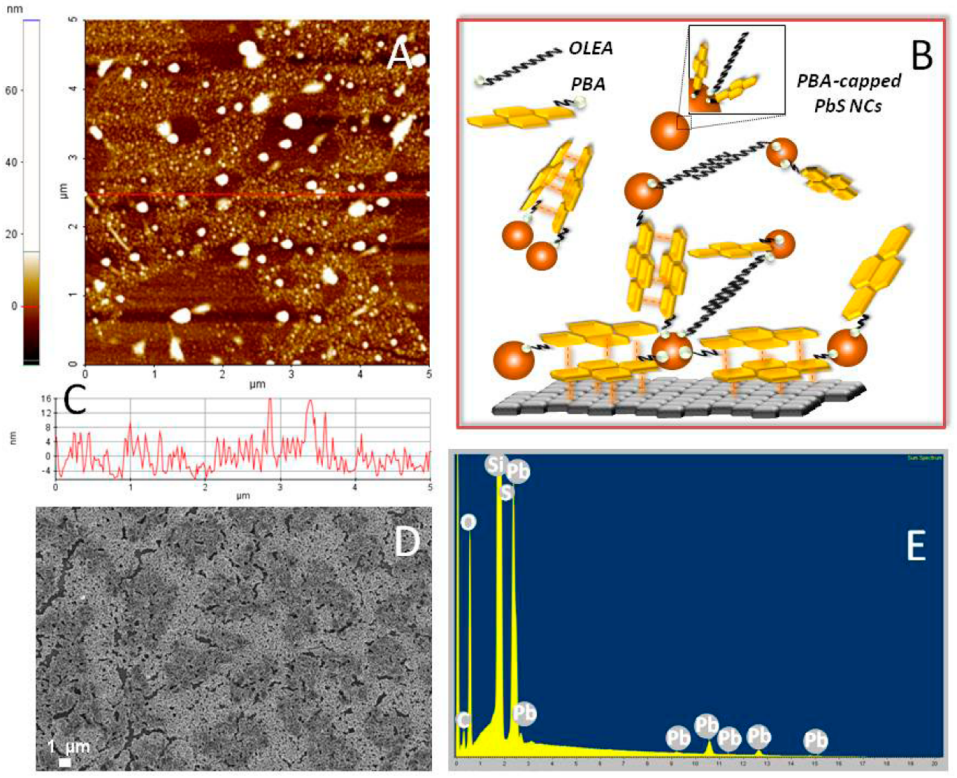

Figure 2. (A) 2D topography AFM images of monolayer CVD graphene functionalized with PBA-capped PbS NCs. (B) Sketch of the PBA-coated PbS NCs anchored to the graphene platform. (C) Cross sectional line profile taken along the red line of panel A. (D) SEM image of the CVD graphene film decorated by PBA-capped PbS NCs supported onto silicon slide and (E) corresponding EDS spectrum in the range 0−20 keV.

A stable dispersion of PBA-coated PbS NCs has been used to functionalize monolayer graphene films supported on SiO_2/Si. The latter have been incubated overnight in the dispersion of the PBA-coated PbS NCs and then rinsed with pure chloroform to remove NCs non specifically adsorbed. This approach, that is of using pyrene as capping ligand directly coordinated to the PbS NC surface for linking chemically the nano-objects to graphene has not been reported in literature so far, to the best of our knowledge. Such an original route specifically aims to avoid aggregation of the aromatic linker by $\pi-\pi$ interactions onto the graphene surface,[26] typically occurring when pyrene is used to anchor at first graphene and then to link nano-objects or biomolecules by specific interactions.[17] This then requires a long purification procedure, without anyway a complete removal of the pyrene stacks from graphene surface. In our approach, based on exposure of graphene to PBA-capped PbS NC solutions, previously purified to remove the free pyrene ligand, the graphene surface interacts specifically with the pyrene molecules anchored to the NC surface.

The morphology of the monolayer CVD graphene has been investigated before and after functionalization with the PBA-capped PbS NCs. Optical microscope image of CVD graphene, as grown on Cu foil, and AFM investigation of CVD graphene upon transfer on SiO_2/Si are reported in Figure S1 of Supporting Information. The investigation demonstrates the complete growth of graphene film, which covers the supporting Cu foil on a large area in merged grains having sizes ranging between 50 and 110 μm^2. The flat and continuous surface of graphene attests for the efficacy of the transferring procedure in retaining continuity of the film and merging among grains.

After treatment with the PBA-coated PbS NCs, the surface morphology of the CVD graphene film supported on SiO_2/Si substrate significantly changes. Panel A of Figure 2 reports the AFM micrograph of the decorated graphene with the corresponding cross sectional line profile in panel C. The surface of the sample results covered by round-shaped nanostructures, closely interconnected, having a thickness of 90 ± 10 nm, that is compatible with multilayers and aggregates of PbS NCs, and a detected lateral size which takes into account the tip convolution effect.[26]

The observed assembly of PbS NCs can be reasonably ascribed to favorable, multiple and cooperative $\pi-\pi$ stacking interactions occurring at the interface between the pyrene linker, capping the PbS NC surface, and the graphene platform[17] (Scheme of Figure 2). In addition, the stacking of the nano-objects in multilayers and in aggregated nanostructures is accounted for by $\pi-\pi$ interactions among the PBA molecules coordinating the NC surface and by interdigitation and possible concomitant cross-linking taking place among the alkyl chains of residual pristine OLEA ligand molecules,[28] as shown by Panel B of Figure 2.

Secondary electron microscopy investigation provides a large area overview of the decorated CVD graphene. Indeed, the substrate appears fully covered by a highly packed and continuous nanoporous multilayer coating (panel D of Figure 2). EDS analysis recorded in the range 0−20 keV (panel E of Figure 2) shows typical features of Pb and S elements, namely the K_α line of S (2.30 keV) and M_α and L_α line of Pb (2.34 and 10.55 keV, respectively). In addition, the chemical mapping (panels B−C in Figure S3 of Supporting Information) clearly demonstrates that the graphene surface is homogeneously coated by Pb and S elements, definitely assigning to PbS NCs the immobilized nanostructures.

DOI: 10.1021/am5081925
ACS Appl. Mater. Interfaces 2015, 7, 4151−4159

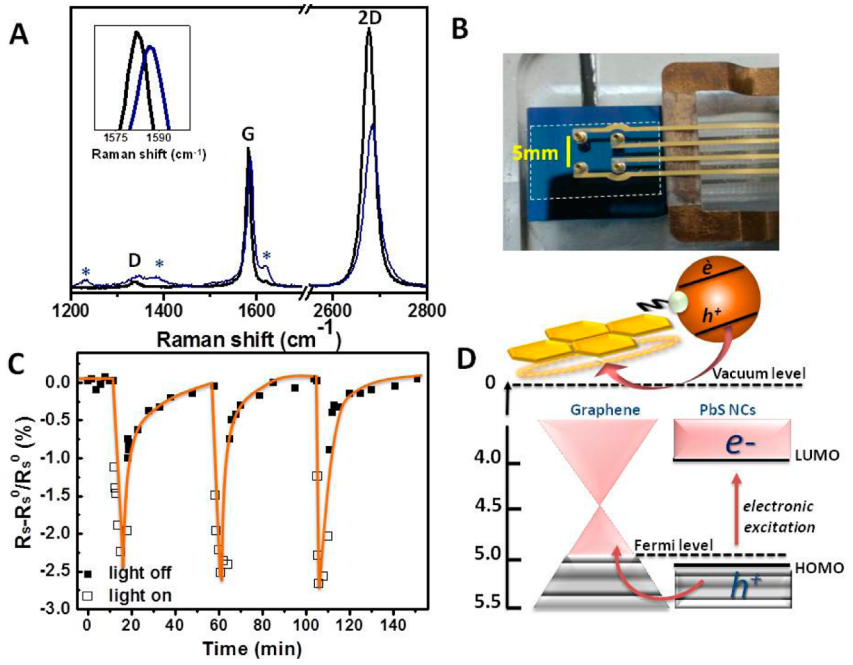

Figure 3. (A) Raman spectra of CVD graphene transferred on SiO_2/Si as bare and functionalized with PBA-capped PbS NCs. (B) Picture of the graphene sheet supported on SiO_2/Si substrate with the 4 Van der Paw probes at a distance of 5 mm from each other. (C) monitoring of the change of the sheet resistance of graphene decorated with PBA-capped PbS NCs under three cycles of light irradiation being Rs^0 = 1000 Ohm × sq^{-1} the sheet resistance in the dark. (D) Sketch of the energy level diagram of graphene and PbS NCs and cartoon of hole stabilization by the pyrene linker capping the NC surface.

The films of CVD graphene decorated by the PBA-capped PbS NCs have been analyzed also by Raman spectroscopy and van der Hall electrical measurements in order to investigate the structural properties of graphene before and after functionalization. Such an investigation can provide a deep insight in possible interactions, as charge or energy transfer processes at the interface, between the organic and the inorganic components, which could be relevant for the effective application of such a functional material in optoelectronic devices.

The Raman spectra of bare CVD graphene after transferring on SiO_2/Si substrate and after decoration with PBA-capped PbS NCs are reported in Figure 3 (black and blue lines of panel A, respectively). The spectrum of the bare graphene sheet on the SiO_2/Si substrate (black line) mirrors that of as-synthesized graphene on Cu foil (see Figure S4 of Supporting Information), attesting for the lack of structural damages coming from the transferring process.

After decoration of graphene with PBA-capped PbS NCs, three new peaks, which are labeled by the asterisk (*) symbol, appear in the spectrum of the hybrid system (blue line). According to the results reported by Shinohara et al.,[29] these features can be attributed to typical intense Raman peaks of pyrene. Moreover, as regards of the Raman spectrum of graphene in the hybrid, it does not shown a substantial change of the D/G ratio (blue line), which attests for the preservation of the conjugated sp^2 carbon lattice after decoration, as expected for a functionalization process promoted by non covalent $\pi-\pi$ stacking interactions. Conversely, the 2D/G ratio of the PbS NC functionalized graphene decreases from 1.8 to 1.1, and these two peaks shift toward higher wavelengths. Namely, the G peak moves from 1582 to 1586 cm^{-1} and the 2D peak goes from 2677 to 2684 cm^{-1}, indicating the occurrence of a change of the graphene electronic state caused by an increase of the hole carrier concentration in the organic platform, as demonstrated by Das and co-workers.[30]

To have a direct prooof of the p-doping effect, Hall measurements of the graphene film, before and after decoration, have been performed by using the cell shown in Panel B of Figure 3.

The large area CVD grown graphene based samples prepared with four-point gold contacts was loaded in the Hall system and electrical measurements were carried out in the Van der Pauw configuration on a sampled area of 5 × 5 mm2. Hall measurements allow to observe for the as grown CVD graphene a p-doping state and to estimate a sheet resistance and hole carrier density of 1000 ± 20 Ohm sq^{-1} and of 2.12 × 10^{13} ± 0.02 × 10^{13} cm^{-2}, respectively. This unintentionally p-doping is originated from oxygen terminations at graphene defects and grain boundaries, interface effects with the substrate and physisorbed contaminants from air, such as O_2, H_2O, and CO_2 that are known to act as p-dopants.[31−33]

After functionalization with PbS NCs the Hall measurements in dark condition show that no substantial change in the electric properties of graphene occurs. Conversely, such parameters modify under light irradiation as shown by panel C of Figure 3, which reports the change of sheet resistance of the graphene coated by the PBA-capped PbS NCs exposed to cycles of irradiation with a white LED light source. The figure shows that, when the light source is turned on, a decrease of sheet resistance of ∼3% occurs (empty square), as a consequence of an increase of the majority charge carries, that are holes. This explains the p-doping evidenced by Raman measurements, owing to the intrusive effect of the laser excitation source on the electronic state of the hybrid system. A slow decrease of the sheet resistance is also observed for irradiation times longer than 5 min, due to thermal effects, although the system is thermostated. These results show a metallic behavior of

DOI: 10.1021/am5081925
ACS Appl. Mater. Interfaces 2015, 7, 4151−4159

graphene which is expected when graphene is in a doping state far from the charge neutrality point (Dirac point).

The reversibility of the process, over several cycles of light illumination, is demonstrated in panel C of Figure 3 (solid square), as well.[34] When the light source is turned off, the graphene sheet resistance recovers to its initial value (Rs^0).

No detectable change of the sheet resistance under light illumination is instead observed for bare graphene and PBA modified graphene as demonstrated by Figure S5 of Supporting Information.

The 3% decrease in sheet resistance of the achieved hybrid is fully in line with the findings of Konstantatos et al.[11] and by Y. Q. Huang et al.[12] These authors have shown for a hybrid material based on OLEA-capped PbS NCs spin-coated on tape exfoliated graphene and then treated with ethanedithiol a photoresponce of 7% and of 2%, respectively measured over a few μm^2 area. Remarkably, here the hybrid system is formed of PbS NCs directly chemically interfaced with graphene by the pyrene ligand and having a photoresponse of 3% measured over a mm^2 region, an area where the contribute of charge carrier trapping at graphene grain boundaries is taken into account.

The photoresponse can be explained by considering the data recently reported.[11,12] Namely, the photon absorption in PbS NCs generates electron−hole pairs which separate under effect of the built-in internal electric field, generated at the interface of the PbS NCs with graphene because of the work function mismatch between the two materials. In particular, the photogenerated holes are transferred to graphene according to the energy level diagram reported in panel D of Figure 3. In such a scheme, the HOMO and LUMO energy levels of the PbS NCs are extrapolated by the values reported in[35] while the energy of the Fermi level of graphene has been estimated from the hole density (n) extrapolated by the Hall measurements with eq 1

$$\mathrm{EF} = -h\nu_{\mathrm{F}}\left(\frac{n}{4\pi}\right)^{1/2} \quad (1)$$

where h and ν_{F} are, respectively, the Planck constant and Fermi velocity.[36]

According to the scheme (Figure 3 panel D), the Fermi level of graphene has an energy higher than the HOMO level of the PbS NCs and hence the photogenerated holes can be transferred to graphene decreasing the sheet resistance.

It is worthwhile to notice that the surface related midgap electron states introduced after capping exchange can contribute in determining the charge transport mechanisms of PBA-coated PbS NCs under illumination, controlling the recombination dynamics of the band-edge charges. Indeed, such low mobility midgap states quickly trap electrons from the band-edge states and let holes in more overlapping and conductive valence band levels dominating photoconduction.[37]

The transfer of photogenerated holes is supposed to be channeled by the short chain aromatic pyrene linker, which coordinates the surface of the PbS NCs concomitantly chemically binding and hence electronically coupling the hybrid components. Such a channeling effect can be accounted for by the fact that, in photoexcited PBA-capped PbS NCs the positive charge can be decoupled from the interior states and stabilized on the π ring system of pyrene in a charge-separated complex and transferred to graphene or other PbS NCs,[38] as shown in panel D of Figure 3. Concomitantly, the network of PbS NCs, provided by the already discussed interligand interactions (panel B of Figure 2), can increase the charge mobility across the NC film, thus favoring a cascade of hole transfer processes also from the nano-objects not directly interfaced with the aromatic platform.

4. CONCLUSIONS

A simple and effective solution-based approach has been developed for manufacturing a hybrid material based on a large area CVD grown monolayer graphene film chemically functionalized with colloidal PbS NCs.

We have exploited the flexibility of the surface chemistry of the NCs to be suitably tailored by organic chemical routes, for replacing the pristine insulating ligand, deriving from the synthetic procedure, with 1-pyrene butyric acid. The functionalized pyrene coordinates the NCs yielding to stable and optically transparent solutions, which mainly retain the optical properties of the nano-objects.

The interface of the hybrid is formed of 1-pyrene butyric acid which anchors the NCs onto graphene by multiple and cooperative $\pi-\pi$ stacking interactions and, by means of the same forces, concomitantly bridge the NCs each other, leading to an highly interconnected nanostructured multilayer coating. After functionalization with PbS NCs, graphene maintains its structure and it results in being doped by a hole transfer channeled by pyrene from the photoexcited PbS NCs. Such an electron communication leads to a material which presents a sheet resistance reduced with respect to that of bare graphene. Thus, the manufactured hybrid can have a relevant potential for integration in solar cells, sensors, photodectors, in tools for bioimaging and in optical information technologies.

In addition, the proposed solution-based functionalization procedure provides a model approach for decorating graphene or nanostructured compounds based on other carbon allotropic forms (i.e., carbon nanotubes, diamond, graphite, fullerenes) with PbS NCs, which may also have a different geometry.

Finally, pyrene ligands, also with different end functional groups, are expected to effectively coordinate nanoparticles having different composition (metal, oxide, chalcogenides), hence diverse interesting properties, thus opening the venue to novel hybrids, with a relevant potential for technological applications.

■ ASSOCIATED CONTENT

Supporting Information

Optical microscopy image and AFM micrographs of CVD graphene on Cu, SEM image of the CVD graphene film decorated by PBA-capped PbS NCs supported onto silicon and corresponding images of chemical mapping of PbS NCs, Raman spectrum of CVD graphene on Cu foil and Lorentzian fitting of the 2D peak, and XRPD data on PbS NC samples, before and after capping exchange procedure. This material is available free of charge via the Internet at http://pubs.acs.org.

■ AUTHOR INFORMATION

Corresponding Author

*Tel:+390805442027. Fax: +390805442128. E-mail: c.ingrosso@ba.ipcf.cnr.it.

Author Contributions

C.I. and G.V.B. contributed equally.

Notes

The authors declare no competing financial interest.

DOI: 10.1021/am5081925
ACS Appl. Mater. Interfaces 2015, 7, 4151−4159

■ ACKNOWLEDGMENTS

This work was partially supported by the National Project 618 (PRIN 2012 prot. 20128ZZS2H), the National 619 Consortium for Material Science and Technology (INSTM) and the National Project Apulia Space (PON03PE-0M67-6). The authors acknowledge funding from the European Community's seventh Framework Programme under grant agreement no. 314578 MEM4WIN (www.mem4win.org), from the Research Project PON R&C 2007−2013 MAAT-Molecular Nanotechnology for Health and Environment (n. PON02_00563_3316357). Giuseppe Chita is acknowledged for collection of the XRPD data.

■ REFERENCES

(1) Novoselov, K. S.; Geim, A. K.; Morozov, S. V.; Jiang, D.; Zhang, Y.; Dubonos, S. V.; Grigorieva, I. V.; Firsov, A. A. Electric Field Effect in Atomically Thin Carbon Films. *Science* **2004**, *306*, 666−669.

(2) Huang, Y.; Liang, J.; Chen, Y. An Overview of the Applications of Graphene-Based Materials in Supercapacitors. *Small* **2012**, *8*, 1805−1834.

(3) Feng, L.; Wu, L.; Qu, X. New Horizons for Diagnostics and Therapeutic Applications of Graphene and Graphene Oxide. *Adv. Mater.* **2013**, *25*, 168−186.

(4) Tu, W.; Zhou, Y. Versatile Graphene-Promoting Photocatalytic Performance of Semiconductors: Basic Principles, Synthesis, Solar Energy Conversion, and Environmental Applications. *Adv. Funct. Mater.* **2013**, *23*, 4996−5008.

(5) Mitta, V. Functional Polymer Nanocomposites with Graphene: A Review. *Macromol. Mater. Eng.* **2014**, *299*, 906−931.

(6) Anandan, S.; Rao, T. N.; Sathish, M.; Rangappa, D.; Honma, I.; Miyauchi, M. Synthesis and Photocatalytic Properties of $LaMnO_3$−Graphene Nanocomposites. *ACS Appl. Mater. Interfaces* **2013**, *5*, 207−212.

(7) Kholmanov, I. N.; Magnuson, C. W.; Aliev, A. E.; Li, H.; Zhang, B.; Suk, J. W.; Zhang, L. L.; Peng, E.; Mousavi, S. H.; Khanikaev, A. B.; Piner, R.; Shvets, G.; Ruoff, R. S. Improved Electrical Conductivity of Graphene Films Integrated with Metal Nanowires. *Nano Lett.* **2012**, *12*, 5679−5683.

(8) Ingrosso, C.; Sardella, E.; Keller, S.; Dohn, S.; Striccoli, M.; Agostiano, A.; Boisen, A.; Curri, M. L. Surface Functionalization of Epoxy-Resist-Based Microcantilevers with Iron Oxide Nanocrystals. *Adv. Mater.* **2010**, *22*, 3288−3292.

(9) Rojas, S.; Gispert, J. D.; Abad, S.; Buaki-Sogo, M.; Victor, M. V.; Garcia, H.; Herance, J. R. In Vivo Biodistribution of Amino-Functionalized Ceria Nanoparticles in Rats Using Positron Emission Tomography. *Mol. Pharmaceutics* **2012**, *9*, 3543−3550.

(10) Curri, M. L.; Comparelli, R.; Striccoli, M.; Agostiano, A. Emerging Methods for Fabricating Functional Structures by Patterning and Assembling Engineered Nanocrystals. *Phys. Chem. Chem. Phys.* **2010**, *12*, 11197−11207.

(11) Konstantatos, G.; Badioli, M.; Gaudreau, L.; Osmond, J.; Bernechea, M.; Garcia de Arquer, F. P.; Gatti, F.; Koppens, F. H. Hybrid Graphene−Quantum Dot Phototransistors with Ultrahigh Gain. *Nat. Nanotechnol.* **2012**, *7*, 363−368.

(12) Huang, Y. Q.; Zhu, R. J.; Kang, N.; Du, J.; Xu, H. Q. Photoelectrical Response of Hybrid Graphene-PbS Quantum Dot Devices. *Appl. Phys. Lett.* **2013**, *103*, No. 143119.

(13) Bi, H.; Huang, F.; Liang, J.; Xie, X.; Jiang, M. Transparent Conductive Graphene Films Synthesized by Ambient Pressure Chemical Vapor Deposition Used as the Front Electrode of CdTe Solar Cells. *Adv. Mater.* **2011**, *23*, 3202−3206.

(14) Cao, A.; Chu, Z. L. S.; Wu, M.; Ye, Z.; Cai, Z.; Chang, Y.; Wang, S.; Gong, Q.; Liu, Y. A Facile One-step Method to Produce Graphene−CdS Quantum Dot Nanocomposites as Promising Optoelectronic Materials. *Adv. Mater.* **2010**, *22*, 103−106.

(15) Chen, Z.; Berciaud, S.; Nuckolls, C.; Heinz, T. F.; Brus, L. E. Energy Transfer from Individual Semiconductor Nanocrystals to Graphene. *ACS Nano* **2010**, *4*, 2964−2968.

(16) Gao, W.; Alemany, L. B.; Ci, L.; Ajayan, P. A. New Insights into the Structure and Reduction of Graphite Oxide. *Nat. Chem.* **2009**, *1*, 403−408.

(17) Katsukis, G.; Malig, J.; Schulz-Drost, C.; Leubner, S.; Jux, N.; Guldi, D. M. Toward Combining Graphene and QDs: Assembling CdTe QDs to Exfoliated Graphite and Nanographene in Water. *ACS Nano* **2012**, *6*, 1915−1924.

(18) Yu, Q.; Jauregui, L. A.; Wu, W.; Colby, R.; Tian, J.; Su, Z.; Cao, H.; Liu, Z.; Pandey, D.; Wei, D.; Chung, T. F.; Peng, P.; Guisinger, N. P.; Stach, E. A.; Bao, J.; Pei, S. S.; Chen, Y. P. Control and Characterization of Individual Grains and Grain Boundaries in Graphene Grown by Chemical Vapour Deposition. *Nat. Mater.* **2011**, *10*, 443−449.

(19) Corricelli, M.; Altamura, D.; De Caro, L.; Guagliardi, A.; Falqui, A.; Genovese, A.; Agostiano, A.; Giannini, C.; Striccoli, M.; Curri, M. L. Self-Organization of Mono- and Bimodal PbS Nanocrystal Populations in Superlattices. *CrystEngComm* **2011**, *13*, 3988−3997.

(20) Moreels, I.; Lambert, K.; Smeets, D.; De Muynck, D.; Nollet, T.; Martins, J. C.; Vanhaecke, F.; Vantomme, A.; Delerue, C.; Allan, G.; Hens, Z. Size-Dependent Optical Properties of Colloidal PbS Quantum Dots. *ACS Nano* **2009**, *3*, 3023−3030.

(21) Hanrat, T.; Veldman, D.; Choi, J. J.; Christova, C. G.; Wienk, M. M.; Janssen, R. A. J. PbSe Nanocrystal Network Formation during Pyridine Ligand Displacement. *ACS Appl. Mater. Interfaces* **2009**, *1*, 244−250.

(22) Law, M.; Luther, J. M.; Hughes, Q. S. B. K.; Perkins, C. L.; Nozik, A. J. Structural, Optical, and Electrical Properties of PbSe Nanocrystal Solids Treated Thermally or with Simple Amines. *J. Am. Chem. Soc.* **2008**, *130*, 5974−5985.

(23) Stouwdam, J. W.; Shan, J.; van Veggel, F.; Pattantyus-Abraham, A. G.; Young, J. F.; Raudsepp, M. Photostability of Colloidal PbSe and PbSe/PbS Core/Shell Nanocrystals in Solution and in the Solid State. *J. Phys. Chem. C* **2007**, *111*, 1086−1092.

(24) Ai, X. C.; Guo, L.; Zou, Y. H.; Li, Q. S.; Zhu, H. S. The Effect of Surface Modification on Femtosecond Optical Kerr Effect of PbS Nanoparticles. *Mater. Lett.* **1999**, *38*, 131−135.

(25) Lokteva, I.; Radychev, N.; Witt, F.; Borchert, H.; Parisi, J.; Kolny-Olesiak, J. Surface Treatment of CdSe Nanoparticles for Application in Hybrid Solar Cells: The Effect of Multiple Ligand Exchange with Pyridine. *J. Phys. Chem. C* **2010**, *114*, 12784−12791.

(26) Haedler, A. T.; Misslitz, H.; Buehlmeyer, C.; Albuquerque, R. Q.; Köhler, A.; Schmidt, H. W. Controlling the π-Stacking Behavior of Pyrene Derivatives: Influence of H-bonding and Steric Effects in Different States of Aggregation. *ChemPhysChem* **2013**, *14*, 1818−1829.

(27) Ward, M. D. Bulk Crystals to Surfaces: Combining X-ray Diffraction and Atomic Force Microscopy to Probe the Structure and Formation of Crystal Interfaces. *Chem. Rev.* **2001**, *101*, 1697−1725.

(28) Odian, G. *Principles of Polymerization*, 4th ed.; Wiley: Hoboken, NJ, 2004; pp 737−738.

(29) Shinohara, H.; Yamakita, Y.; Ohno, K. Raman Spectra of Polycyclic Aromatic Hydrocarbons. Comparison of Calculated Raman Intensity Distributions with Observed Spectra for Naphthalene, Anthracene, Pyrene, and Perylene. *J. Mol. Struct.* **1998**, *442*, 221−234.

(30) Das, A.; Pisana, S.; Chakraborty, B.; Piscanec, S.; Saha, S. K.; Waghmare, U. V.; Novoselov, K. S.; Krishnamurthy, H. R.; Geim, A. K.; Ferrari, A. C.; Sood, A. K. Monitoring Dopants by Raman Scattering in an Electrochemically Top-Gated Graphene Transistor. *Nat. Nanotechnol.* **2008**, *3*, 210−215.

(31) Bianco, G. V.; Losurdo, M.; Giangregorio, M. M.; Capezzuto, P.; Bruno, G. Exploring and Rationalising Effective n-Doping of Large Area CVD-Graphene by NH_3. *Phys. Chem. Chem. Phys.* **2014**, *16*, 3632−3639.

(32) Martin, J.; Akerman, N.; Ulbricht, G.; Lohmann, T.; Smet, J. H.; Von Klitzing, K.; Yacoby, A. Observation of Electron−Hole Puddles in Graphene using a Scanning Single-Electron Transistor. *Nat. Phys.* **2008**, *4*, 144−148.

DOI: 10.1021/am5081925
ACS Appl. Mater. Interfaces 2015, 7, 4151−4159

(33) Ni, Z. H.; Wang, H. M.; Luo, Z. Q.; Wang, Y. Y.; Yu, T.; Wu, Y. H.; Shen, Z. X. The Effect of Vacuum Annealing on Graphene. *J. Raman Spectrosc.* **2010**, *41*, 479−483.
(34) Heo, J.; Chung, H. J.; Lee, S. H.; Yang, H.; Seo, D. H.; Shin, J. K.; Chung, U. I.; Se, S.; Hwang, E. H.; Sarma, S. D. Nonmonotonic Temperature Dependent Transport in Graphene Grown by Chemical Vapor Deposition. *Phys. Rev. B* **2011**, *84*, 035421−035427.
(35) Hyun, B. R.; Zhong, Y. W.; Bartnik, A. C.; Sun, L.; Abrun, H. D.; Wise, F. W.; Goodreau, J. D.; Matthews, J. R.; Leslie, T. M.; Borrelli, N. F. Electron Injection from Colloidal PbS Quantum Dots into Titanium Dioxide Nanoparticles. *ACS Nano* **2008**, *11*, 2206−2212.
(36) Liu, L.; Ryu, S.; Tomasik, M. R.; Stolyarova, E.; Jung, N.; Hybertsen, M. S.; Steigerwald, M. L.; Brus, L. E.; Flynn, G. W. Graphene Oxidation: Thickness-Dependent Etching and Strong Chemical Doping. *Nano Lett.* **2008**, *8*, 1965−1970.
(37) Nagpa, P.; Klimov, V. I. Role of Mid-Gap States in Charge Transport and Photoconductivity in Semiconductor Nanocrystal Films. *Nat. Commun.* **2011**, *2*, 486.
(38) Guyot-Sionnest, P.; Shim, M.; Matranga, C.; Hines, M. Intraband Relaxation in CdSe Quantum Dots. *Phys. Rev. B* **1999**, *60*, No. R2181.

DOI: 10.1021/am5081925
ACS Appl. Mater. Interfaces 2015, 7, 4151−4159